

Dependence of peculiar velocity on the host properties of the gravitational wave sources and its impact on the measurement of Hubble constant

Harshank Nimonkar¹^{*}, Suvodip Mukherjee²[†]

¹Department of Physics, St. Xavier's College, 5, Mahapalika Marg, Mumbai 400001, India

²Department of Astronomy & Astrophysics, Tata Institute of Fundamental Research, 1, Homi Bhabha Road, Colaba, Mumbai 400005, India

Accepted XXX. Received YYY; in original form ZZZ

ABSTRACT

Accurate measurement of the Hubble constant from standard sirens such as the gravitational wave (GW) sources with electromagnetic counterparts relies on the robust peculiar velocity correction of the redshift of the host galaxy. We show in this work that the peculiar velocity of the host galaxies exhibits a correlation with the properties of the host galaxy primarily such as its stellar mass and this correlation also evolves with redshift. As the galaxies of higher stellar mass tend to form in galaxies with higher halo masses which are located in spatial regions having a non-linear fluctuation in the density field of the matter distribution, the root mean square (RMS) peculiar velocity of more massive galaxies is higher. As a result, depending on the formation channel of the binary compact objects, the peculiar velocity contamination to the galaxies will be different. The variation in the peculiar velocity of the host galaxies can lead to a significant variation in the estimation of the Hubble constant inferred using sources such as Binary Neutron Stars (BNSs). For the network of GW detectors such as LIGO-Virgo-KAGRA (LVK), LVK+LIGO-India, and Cosmic Explorer+Einstein Telescope, the variation in the precision of Hubble constant inferred from 10 bright siren events can vary from $\sim 5.4 - 6\%$, $\sim 4.5 - 5.3\%$ and $\sim 1.1 - 2.7\%$ respectively. The impact of such a correlation between peculiar velocity and stellar mass on the inference of the Hubble constant is not only limited to GW sources but also applicable to type-Ia supernovae.

Key words: Galaxy: kinematics and dynamics – gravitational waves – neutron star mergers

1 INTRODUCTION:

Gravitational wave (GW) sources such as binary neutron star (BNS), binary black hole (BBH), and neutron star-black hole (NSBH) systems (Abbott et al. 2016b, 2017a, 2021b) are called standard sirens as they offer a unique advantage by providing an independent and accurate measure of their luminosity distance to the source (Schutz 1986). However, due to the nature of GW observations, there is an inherent degeneracy between the luminosity distance and the inclination angle, which is the orientation of the orbital plane with respect to the observer. The degeneracy between these two parameters presents a challenge in accurately determining the astrophysical properties of the sources solely based on GW observations unless the distance-inclination angle degeneracy can be lifted by measuring the two polarizations of GW, using higher order modes for asymmetric mass systems, or improving the inference of inclination angle using observations from electromagnetic (EM) bands (Holz & Hughes 2005; Nissanke et al. 2010, 2013; Mooley et al. 2018a; Hotokezaka et al. 2018; Mukherjee et al. 2020a).

Bright standard sirens having an observable EM counterpart, allow for an independent measurement of the redshift of the host galaxy which can be used along with the measured luminosity distance to measure cosmological parameters that impact the expansion history

of the Universe such as the Hubble constant (H_0) (Schutz 1986; Holz & Hughes 2005; Nissanke et al. 2010, 2013; Mooley et al. 2018a; Hotokezaka et al. 2018; Chen et al. 2018; Feeney et al. 2019; Mortlock et al. 2019). Such measurements are performed for the event GW170817 by combining the measurement of luminosity distance and redshift (Abbott et al. 2017b). A further improvement in the measurement of H_0 was possible by including the constraints on inclination angle from jet measurement (Hotokezaka et al. 2018). This measurement was further revised by including a better measurement of peculiar velocity (Mukherjee et al. 2020a; Howlett & Davis 2020; Nicolaou et al. 2020). Another GW event GW190521 (Abbott et al. 2020b) with tentative EM association made it possible to obtain a weak measurement on H_0 (Mukherjee et al. 2021b; Gayathri et al. 2021; Chen et al. 2022).

Along with bright siren measurement, measurements from dark standard sirens made using statistical-host identification technique (Soares-Santos et al. 2019; Fishbach et al. 2019; Abbott et al. 2021b, 2023; Palmese et al. 2023; Gair et al. 2023), mass distribution (Mastroianni et al. 2021a; Leyde et al. 2022; Karathanasis et al. 2023) and more recently by using the spatial clustering of the GW sources with galaxies (Mukherjee et al. 2022) using cross-correlation method (Oguri 2016; Mukherjee et al. 2020b, 2021a; Diaz & Mukherjee 2021) have emerged as an independent probe having the potential to reach the required percent level precision on H_0 , thus advancing towards resolving the well established Hubble tension (Hinshaw et al. 2013; Planck Collaboration et al. 2014, 2016; Wong et al. 2019;

* harshank.nimonkar@xaviers.edu.in; nimonkar.harshank@gmail.com

† suvodip@tifr.res.in

Planck Collaboration et al. 2021; Riess et al. 2022; Abdalla et al. 2022).

In an isotropically expanding universe (Lemaître 1927; Hubble 1929; Lemaître & Eddington 1931), the gravitational instability within large-scale structures leads to deviations from the smooth Hubble flow, introducing irregularities in the motion of the host galaxies of GW sources. Consequently, these galaxies acquire an additional velocity component beyond their recessional velocity (due to the Hubble flow). The additional velocity component of the host galaxy of a GW source, called peculiar velocity, contaminates the redshift measurements from the EM counterpart. The contribution from the peculiar velocity (few hundreds of km s^{-1}) to the motion of a GW host is significant up to a redshift of $z = 0.05$ ($\approx 15,000 \text{ km s}^{-1}$). The contamination from individual sources degrades the accuracy and precision in the measurement of H_0 if not accounted for appropriately (Mukherjee et al. 2020a; Howlett & Davis 2020; Nicolaou et al. 2020).

As we show in the following sections, the peculiar velocity dispersion depends on the property of the galaxy such as the stellar mass. The galaxies with higher stellar mass tend to have a larger peculiar velocity dispersion than the sources with lower stellar mass. As a result, depending on the formation of the GW sources in galaxies with higher or lower stellar mass, they will have different amounts of contamination. With the current sensitivities of the ground-based GW detectors, we expect confident bright siren detection up to $\sim 200 \text{ Mpc}$ (Abbott et al. 2020a) which makes it a matter of concern to understand the role of their host properties and the possible contamination from the peculiar velocity that can impact the estimation of H_0 .

The paper is structured as follows, in section 2, we discuss the motivation behind this work, followed by a brief review of the peculiar velocity formalism employed in this work in section 3. In section 4, we discuss our approach toward modeling a population of bright sirens. In section 5, we simulate bright siren events in these populations of galaxies considering different ground-based GW detector configurations followed by a Bayesian parameter estimation of the luminosity distance and inclination angle of the simulated GW sources. Finally in section 6 we summarize the work and discuss future outlook.

2 MOTIVATION

The presence of perturbations in the matter density leads to physical motion of the galaxies with respect to the cosmic rest frame, known as the peculiar velocity. The study of peculiar velocities has implications for our understanding of dark matter and dark energy and for interpreting observed cosmological phenomena such as redshift space distortions (Fry & Gaztanaga 1994; Song & Percival 2009; Hudson & Turnbull 2012; Zheng et al. 2013; Kim & Linder 2020; Cuesta-Lazaro et al. 2020; Adams & Blake 2020; Turner et al. 2022).

The total velocity of the host galaxy of a GW source is the sum of the velocity due to Hubble flow, the peculiar velocity, and the velocity of the observer. Thus, in the expansion frame of reference, the peculiar velocity of the host galaxy v_p is related to the velocity of the source \vec{v}_s and that of the observer \vec{v}_o as

$$v_p = (\vec{v}_s - \vec{v}_o) \cdot \hat{n} \quad (1)$$

where v_p is directed along the line of sight denoted by \hat{n} . A positive value of v_p implies that the host galaxy is moving away from the observer. The difference in velocities of the source and the observer leads to a difference in the observed and true (cosmological) redshift

as,

$$(1 + z_{\text{obs}}) = (1 + z_{\text{true}}) \left(1 + \frac{v_p}{c}\right). \quad (2)$$

For a GW source at a cosmological redshift z_{true} , its luminosity distance is given via the distance-redshift relation as,

$$d_L = \frac{c(1 + z_{\text{true}})}{H_0} \int_0^{z_{\text{true}}} \frac{dz}{E(z)}, \quad (3)$$

where the term $E(z) = \sqrt{\Omega_m(1+z)^3 + (1 - \Omega_m)}$ is the ratio of the Hubble parameter ($H(z)$) to the Hubble constant H_0 , written in terms of matter density Ω_m for a flat Λ CDM cosmological model. However, for low redshifts, $H(z)$ is nearly constant. Hence eq. 3 simplifies greatly to,

$$d_L = \frac{cz_{\text{true}}}{H_0}, \quad (4)$$

thus becoming independent of the cosmological model. Incorporating the peculiar velocity (eq. 2) into the luminosity distance (eq. 4), we get,

$$d_L = \frac{cz_{\text{obs}} - v_p}{H_0}. \quad (5)$$

Thus, for a bright siren event, with the d_L estimated from the GW data and z_{obs} estimated from the EM counterpart, the peculiar velocity v_p can lead to a bias in the inferred value of H_0 if not accounted for and corrected appropriately.

The peculiar velocity of the galaxies depends on the environment where they are forming. Galaxies that are forming in the dense environment and in large galaxy halo will exhibit larger peculiar velocity (with both linear and non-linear components) (Fry & Gaztanaga 1994; Song & Percival 2009; Lavaux & Hudson 2011; Hudson & Turnbull 2012; Zheng et al. 2013; Cuesta-Lazaro et al. 2020). The formation of galaxies in massive halos in a dense environment will have different astrophysical properties such as stellar mass, and star formation rate (see a review by Wechsler & Tinker 2018a) and as a result, there will exist a correlation between the galaxy properties such as stellar mass and peculiar velocity of the galaxies.

Along with the connection between the galaxies and halos, the formation of the GW sources is related to the properties of galaxies and hence also properties of the halo. Formation of bright standard sirens and their merging depends on the formation channel and properties of the galaxies such as its stellar mass, star formation rate (Perna et al. 2022; Santoliquido et al. 2022, 2023). So, depending on the underlying population of the host of GW sources, the halo property of the galaxies and hence the peculiar velocity contamination will be different. In this work, we are interested to show the dependence of the peculiar velocity on the astrophysical property of the host galaxies such as its stellar mass M_\star and how the interplay between the underlying GW source population and stellar mass can lead to different amount of contamination from peculiar velocity to the host of the GW sources. A GW source population dependent peculiar velocity contamination will lead to a population dependent impact on the inference of the value of Hubble constant from the low redshift sources. We show the impact of stellar-mass dependent peculiar velocity contamination on the value of Hubble constant for the ongoing and upcoming GW surveys and how to mitigate such effects from future observations with the network of GW detectors such as LIGO+Virgo+KAGRA (LVK) (Gregory 2010; Aso et al. 2013; Abbott et al. 2018; Acernese et al. 2014; Aasi et al. 2015; Abbott et al. 2016a; Akutsu et al. 2021), LVK+LIGO-India (LVKI) (Unnikrishnan 2013; Saleem et al. 2022), and Cosmic Explorer+Einstein Telescope (CE+ET) (Punturo et al. 2010; Maggiore et al. 2020; Hall & Evans 2019; Evans et al. 2021a; Adhikari et al. 2022).

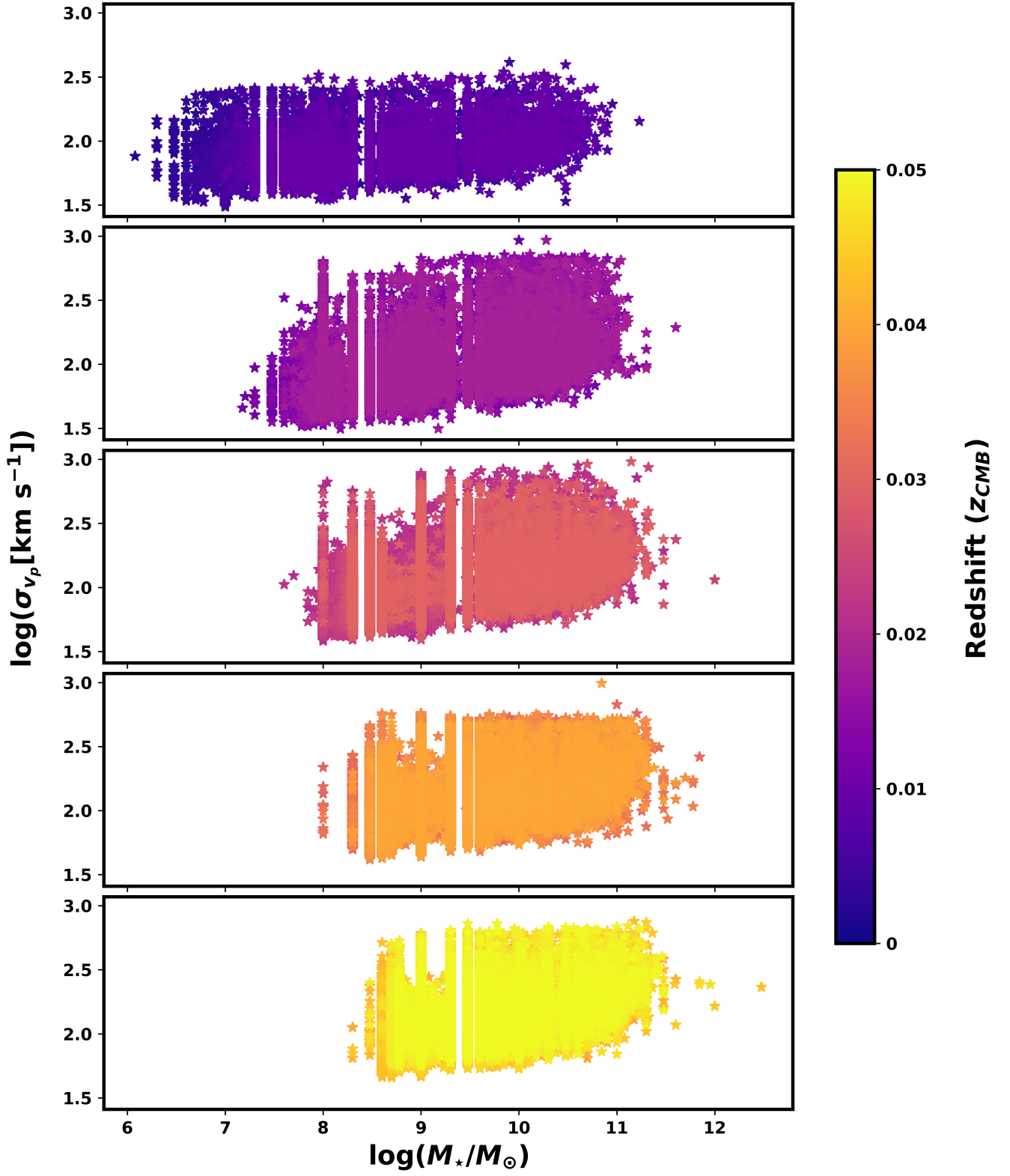


Figure 1. This plot is the entire filtered GLADE+ catalog divided into five subplots based on five redshift bins showing the velocity dispersion as a function of stellar mass.

3 MODELING THE IMPACT OF PECULIAR VELOCITY

Efforts for estimating the cosmic peculiar velocity field has spanned decades of extensive research (Kaiser et al. 1991; Shaya et al. 1992; Hudson 1994; Davis et al. 1996; Branchini et al. 1999, 2002; Nusser et al. 2001; Sheth & Diaferio 2001; Hudson et al. 2004; Radburn-Smith et al. 2004; Pike & Hudson 2005; Lavaux & Hudson 2011; Davis et al. 2011; Ma et al. 2012; Turnbull et al. 2012; Carrick et al. 2015; Mukherjee et al. 2021b). In the linear regime, where the density fluctuations are very small, the resulting velocity dispersions are underestimated (Mukherjee et al. 2021b). The peculiar velocity model by Sheth & Diaferio (2001) accounts for the non-linearities in the density field.

Assuming that all dark matter particles lie in a spherical virialized halo, Sheth & Diaferio (2001) proposed that the peculiar velocity, \vec{v}_p , has two components,

$$\vec{v}_p = \vec{v}_{halo} + \vec{v}_{vir}, \quad (6)$$

where \vec{v}_{vir} is the higher order term which represents the virial motion of a dark matter particle around the center of mass of parent halo, and \vec{v}_{halo} represents the motion of the center of mass of the halo. The linear component arises from the bulk flow of a group or cluster while the non-linear term results from the non-linear interactions between galaxies within a cluster. Hence the velocity dispersion for the non-linear component depends upon the mass of the parent halo, $\sigma_{vir} \propto m^{1/3}$. The proportionality constant, obtained from the relations given by Bryan & Norman (1998), sets the dispersion for the non-linear term as

$$\sigma_{vir} = 476 g_{\sigma} (\Delta_{nl} E(z)^2)^{1/6} \left(\frac{m}{10^{15} M_{\odot} / h} \right)^{1/3} \text{ km s}^{-1}, \quad (7)$$

for a galaxy with a halo of mass m in a region with non-linear overdensity contrast Δ_{nl} approximated by,

$$\Delta_{nl} = 18\pi^2 + 60x - 32x^2, \quad (8)$$

where $x = \Omega_m (1+z)^3 / E(z)^2 - 1$ and the term $g_{\sigma} = 0.9$ is a normalization factor (Sheth & Diaferio 2001). The fitting form for the bulk flow is obtained by extrapolating root-mean-square velocities of the dark matter particles from peaks in the velocity power spectrum from Colberg et al. (2000).

Our work relies on the peculiar velocity estimates from the technique developed by Mukherjee et al. (2021b) which utilizes the BORG (Bayesian Origin Reconstruction from Galaxies) formalism (Jasche & Wandelt 2013; Jasche, J. & Lavaux, G. 2019). By fitting a dynamical structure formation model to observed galaxies in cosmological surveys, the BORG method infers a physically feasible and probabilistic model of the three-dimensional cosmic matter distribution, providing the linear and partially non-linear components of the velocity field. The BORG algorithm accounts for unknown galaxy bias and incorporates selection and evolutionary effects while providing the velocity field as part of the dynamical model. BORG method provides a numerical approximation of the posterior distribution of the parameters in a spatial grid of 256^3 values with a spatial resolution of $2.64 \text{ Mpc } h^{-1}$ for the initial conditions plus the bias parameters. The dark matter particle's initial and final positions are provided for each sample of the posterior, allowing for the estimation of the velocity field using the Simplex-in-Cell estimator.

The implementation of BORG framework has been discussed extensively in Mukherjee et al. (2021b). BORG reconstructs the initial density field and simulates the evolution of the density fluctuations under gravity via linear perturbation theory to estimate the v_{halo} (linear) component. This component paired with the non-linear term (eq. 7) together forms the peculiar velocity field.

In order to explicate the correlation between the peculiar velocity of host galaxies of GW sources and their properties, we consider real galaxies from the GLADE+ galaxy catalog (Dálya et al. 2022) (more details in section 4.3). GLADE+ catalog consists of the redshifts of the galaxies corrected for their peculiar motions using the BORG formalism discussed above. By filtering the catalog to include galaxies with $z_{\text{true}} \leq 0.05$, we examine the distribution of the peculiar velocity as a function of stellar mass.

Fig. 1 shows the distribution of the log of peculiar velocity dispersions as a function of the log-stellar mass of all galaxies up to redshift $z = 0.05$ from the GLADE+ galaxy catalog. The total distribution is divided into five sub-distributions based on five redshift ranges ranging from $z = 0.01$ to $z = 0.05$. As indicated by the color bar, the topmost panel shows the distribution for $0 < z \leq 0.01$, the second panel shows the same for $0.01 < z \leq 0.02$, and so on. As we proceed from the top panel towards the bottom, more galaxies are detected with higher stellar mass. This is because the galaxies that are further away with less stellar mass are fainter and were not detected in a magnitude-limited survey. The number of galaxies detected is also large as the comoving volume of the Universe at high redshift is large. Regardless of the redshift range, an increase in the stellar mass leads to an increase in the peculiar velocity dispersion.

To show the dependence of the dispersion of the peculiar velocity on the host property of the galaxy, we show a violin plot in Fig. 2, which represents the median distribution of the log of the peculiar velocity dispersion as a function of log-stellar mass of galaxies. Here the galaxies in each stellar mass bin are divided into two redshift bins, z between 0 and 0.025 and z from 0.025 up to 0.05. For each stellar mass bin, the orange curves represent the distributions for galaxies in the lower z bin ($0 < z \leq 0.025$), and the purple ones represent those in the higher z bin ($0.025 < z \leq 0.05$). The first three violins do not exhibit a purple posterior which indicates that for those stellar mass bins, there are no galaxies detected in the higher z bin as low-mass galaxies are not bright enough to be detected at higher redshifts. This can be validated from the lower panels of Fig. 1. Overall, we see an increasing trend in the median distribution of log-peculiar velocity dispersion with an increase in the order of the stellar mass in both the redshift bins, which indicates a population-dependent peculiar velocity contamination. In every stellar mass bin, the orange posteriors are skewed towards a lower value of peculiar velocity as compared to the purple posteriors which indicates a redshift-dependent contamination from peculiar velocity. Previous studies on other datasets have also found a similar trend of increase in the velocity dispersion with an increase in the stellar mass (Sohn et al. 2017; Napolitano et al. 2020). The velocity trend observed from GLADE+ agrees with previous findings. The key summary from this section is that the underlying peculiar velocity dispersion depends on the stellar mass and host redshift of the sources. As a result, whether most GW sources are hosted in galaxies with higher (or lower) stellar mass, their peculiar velocity contamination will be different. It is important to note here that this impact can be also important for standard candles. These sources can also exhibit a population-dependent peculiar velocity contamination. We will explore this in a future work.

4 MODELING GW SOURCE POPULATION FOR BRIGHT SIRENS

Bright standard sirens have an observable EM counterpart and hence are expected to be detected at low redshifts. The contribution of peculiar velocity is significant typically up to $z = 0.05$ (Mukherjee et al. 2020a). Our work focuses on low redshift bright sirens, particularly

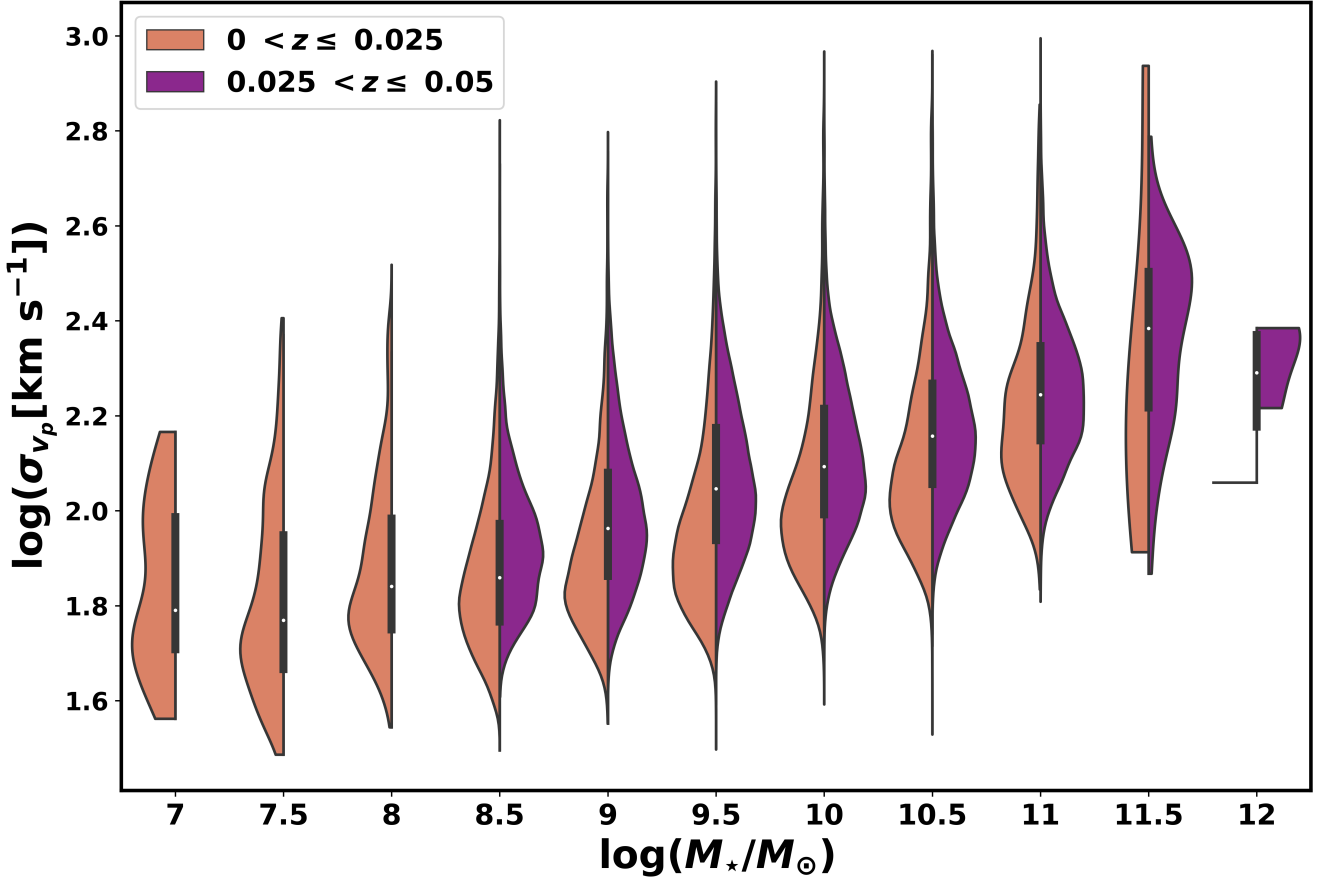


Figure 2. The median distribution of the log-peculiar velocity as a function of log-stellar mass for all galaxies up to redshift of 0.05 from the GLADE+ catalog. The two posteriors in each violin represent the two redshift bins.

BNS mergers. To probe the impact of the host properties of BNSs, it is essential to model their population appropriately. The merger rate of compact binaries plays a key role in this aspect. The merger rate for compact binaries as a function of some physical property like stellar mass or redshift gives the probability distribution for their host galaxies with respect to that property.

4.1 Merger rate density distribution for BNS hosts

According to our current understanding of galaxy formation, the formation and growth of a galaxy depends on the halo properties [a review article on this topic (Wechsler & Tinker 2018b)]. The relation between the halo-mass and stellar mass in a galaxy as a function of redshift is a useful indicator for the formation of galaxies. Almost all properties of galaxies are strongly influenced by their stellar mass (Kauffmann et al. 2004; Taylor et al. 2011). High (low) mass galaxies typically exhibit old (young) stellar populations, high (low) mass-to-light ratios, and low (high) star formation rates (Kauffmann et al. 2003b). There is also a tight correlation between stellar mass and the metal content in the gas phase of emission-line galaxies (Kauffmann et al. 2003a; Tremonti et al. 2004) indicating that the amount of metals in a galaxy is closely connected to its stellar mass.

The formation of BNSs in a galaxy depends on the halo mass and also the stellar properties of a galaxy such as stellar mass, star formation rate, stellar metallicity (Perna et al. 2022; Santoliquido

et al. 2022, 2023). As a result, the merger rate of BNSs at a redshift depends on the host galaxy properties such as the stellar mass, which in turn also depends on the halo-mass. The properties of galaxies in which binary compact objects (BCOs) form (called formation galaxies) can significantly vary from those in which BCOs merge (called host galaxies). The properties of the host galaxy and formation galaxy can differ significantly depending on the growth history of the galaxy and also the delay time between the formation of the stars and the merging of a BNS. For instance, the formation and evolution of a BNS system span 10^6 years (1 Myr) to 10^9 years (1 Gyr) before it finally merges. Throughout this timescale, its formation galaxy can be subjected to significant alterations via chemical evolution or even galaxy-galaxy merger resulting in its host galaxy having properties dissimilar to its formation galaxy.

To model the host properties of GW sources, Santoliquido et al. (2022) simulated the mergers of compact binaries using binary population models for their progenitors while considering the evolution and possible mergers of their host galaxies across different cosmic timescales. The host properties such as the galaxy stellar mass, metallicity and star formation rate (SFR) are assumed to be following either the mass metallicity relation (MZR) (Tremonti et al. 2004; Kewley & Ellison 2008; Maiolino, R. et al. 2008; Mannucci et al. 2009; Mag-nelli, B. et al. 2012; Zahid et al. 2014; Genzel et al. 2015; Sanders et al. 2019) or the fundamental metallicity relation (FMR) (Mannucci et al. 2010, 2011; Hunt et al. 2012, 2016; Curti et al. 2019;

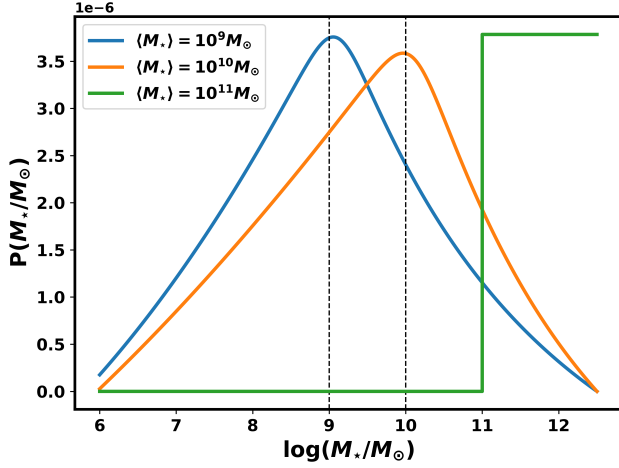


Figure 3. The probability distributions over log-stellar mass used to sample three different populations of galaxies from the filtered GLADE+ catalog. The blue and orange curves are fitted with a broken power law with the given parameters. The green line is a step function used to restrict samples to high-mass galaxies.

Sanders et al. 2019). As seen in section 3, the peculiar velocity dispersion depends upon the mass of the parent halo of the host galaxy and hence on their stellar mass content (see Fig. 2). To model the source population, we adapt from Santoliquido et al. the distribution of BNS merger rate density as a function of the host stellar mass for local galaxies assuming FMR. Following their log-normal merger rate density distribution (Santoliquido et al. Page 9, figure 8: BNS $\alpha 1$ FMR), we fit a broken power law (more in section 4.3) using the following equation

$$f(dm) \propto \left(\frac{dm}{m_{\text{break}}}\right)^{\alpha_1} \left\{ \frac{1}{2} \left(1 + \left(\frac{dm}{m_{\text{break}}}\right)^{\frac{1}{\Delta}} \right) \right\}^{(\alpha_2 - \alpha_1)\Delta} \quad (9)$$

where $dm = \text{dlog}(M_{\star}/M_{\odot})$, m_{break} is the pivotal point of change of slope, α_1 and α_2 are the power law indices and Δ is the smoothness parameter. Normalizing the above equation for the probability density function (PDF), we get the probability densities for BNS host galaxies across a log-stellar mass range of [6, 13] which gives the probability that a GW event detected by a detector is emitted by a coalescing BNS located in a galaxy that has log-stellar mass given by the log-mass bin dm . The value of m_{break} in the work by Santoliquido et al. (2022) is approximately $10^{10.5} M_{\odot}$ which implies that galaxies with a stellar mass of the order of $10^{10} M_{\odot}$ are estimated to have the largest number of BNS mergers per $\text{Gpc}^3 \text{yr}^{-1}$ (following the merger rate distribution).

4.2 Redshift dependent merger rate model

Having constructed a model describing the distribution of stellar masses across the galaxies hosting BNS systems, the next stage involves modeling the redshifts associated with these galaxies. The number of Compact Binary Coalescing (CBC) events per unit redshift per unit observation time is estimated using Karathanasis et al. (2022) as

$$\frac{dN_{\text{GW}}}{dz dt} = \frac{R(z)}{1+z} \frac{dV_c}{dz}(\theta_{\Lambda\text{CDM}}); \quad (10)$$

where $\frac{dV_c}{dz}(\theta_{\Lambda\text{CDM}})$ is the comoving volume at redshift z for the cosmological parameters denoted by $\theta_{\Lambda\text{CDM}}$ for the flat- Λ CDM model

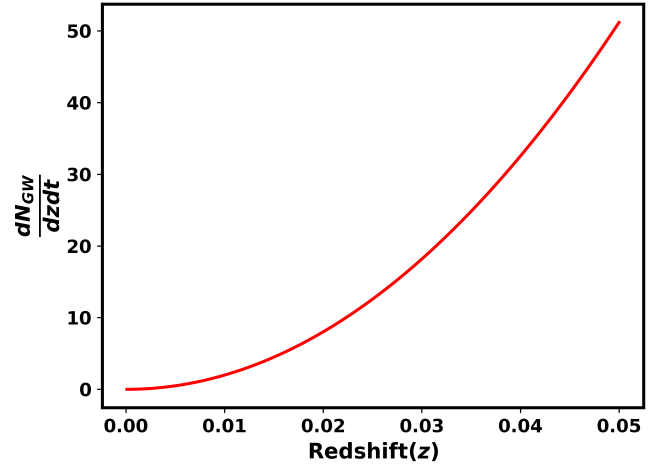


Figure 4. The number of BNS coalescing events per redshift bin dz for a given observation time dt . The curve shows the distribution of the host galaxies of GW sources up to a redshift $z = 0.05$.

and $R(z)$ is the redshift evolution of the merger rate for different delay time distributions

$$R(z) = R_0 \int_z^{\infty} P(t_d | t_d^{\text{min}}, t_d^{\text{max}}, d) R_{\text{SFR}}(z_m) \frac{dt}{dz_m} dz_m, \quad (11)$$

where $P(t_d | t_d^{\text{min}}, t_d^{\text{max}}, d) = (t_d)^{-d}$ is the probability distribution of the delay time (t_d) given the power law index d ; $R_{\text{SFR}}(z)$ is the star-formation rate at redshift z (Madau & Dickinson 2014) and R_0 is the merger rate at redshift $z = 0$. The minimum and maximum time delay is given in terms of the lookback time and the local merger rate R_0 for BNS is inferred by The LIGO Scientific Collaboration et al. (2022) between $10 \text{ Gpc}^{-3} \text{yr}^{-1}$ and $1700 \text{ Gpc}^{-3} \text{yr}^{-1}$. Our work assumes a fiducial local merger rate of $R_0 = 20 \text{ Gpc}^{-3} \text{yr}^{-1}$. Hence eq. (10) gives the number of BNS coalescing events per unit redshift per unit observation time. This gives the distribution of BNS host galaxies per redshift bin dz for a given observation time dt . Integrating the eq. (10) for a given observation time (including the detector duty cycle) and the redshift range gives the total number of BNS events up to that redshift. Hence, for redshifts up to 0.05, the distribution of BNS host galaxies is shown in Fig. 4. In this analysis we consider the BNS to follow the Madau-Dickinson SFR (Madau & Dickinson 2014) with a negligible minimum delay time.

4.3 GLADE+ galaxy catalog

Using the mass distribution model of BNS and merger rate model, we choose the host galaxies of BNS from the GLADE+ galaxy catalog (Dálya et al. 2022). In order to do so, we consider the distribution of host galaxies of BNSs across the stellar mass range of $10^6 M_{\odot}$ to $10^{12} M_{\odot}$ along with their distribution across redshift up to $z = 0.05$. The GLADE+ galaxy catalog is constructed with the purpose of optimizing multi-messenger searches by facilitating the process of sky localization for EM follow-up. The catalog contains 22.5 million galaxies and 7,50,000 quasars. It consists of the redshifts of the galaxies in the CMB frame, their stellar masses, and their peculiar velocity uncertainties estimated from the BORG framework (Mukherjee et al. 2021b; Jasche & Wandelt 2013; Jasche, J. & Lavaux, G. 2019). The redshift flag (z_{flag}) with a value of 1 indicates that the redshift of the galaxy in the CMB frame is corrected for the peculiar velocity bias, i.e., $z_{\text{CMB}} = z_{\text{true}}$. Hence, to garner a population of potential

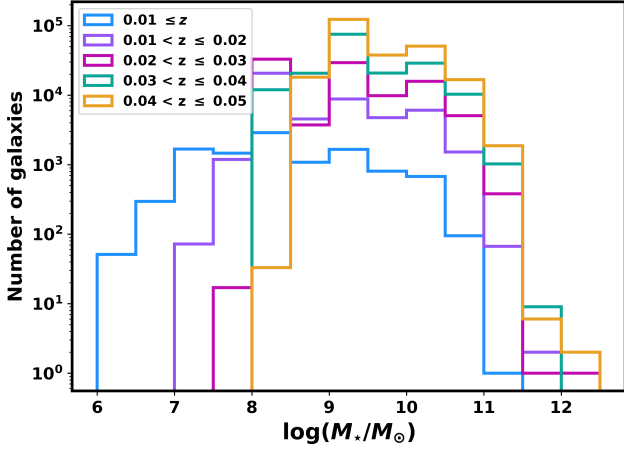


Figure 5. Distribution of galaxies from the filtered GLADE+ catalog as a function of their log-stellar mass. The distribution includes galaxies up to $z = 0.05$ in 5 bins.

BNS host galaxies, we filter the GLADE+ catalog by applying the following conditions:

- $z_{\text{CMB}} \leq 0.05$,
- $M_{\star} \neq \text{'null'}$,
- $z_{\text{flag}} = 1$.

With these restrictions, we get a subset of GLADE+ (henceforth called ‘filtered GLADE+’) containing 572558 galaxies. The filtered GLADE+ contains galaxies up to $z \leq 0.05$ corrected for their peculiar velocity bias and transformed to the CMB frame. It also contains the stellar masses (M_{\star}), peculiar velocity dispersion (σ_{v_p}), and the sky location (right ascension (RA) and Declination (Dec)) of galaxies up to $z_{\text{CMB}} = 0.05$. Fig. 5 shows the distribution of galaxies from the filtered GLADE+ catalog as a function of the stellar mass.

To understand the impact of the host galaxy properties of BNSs on the peculiar velocity and subsequently, on the inference of H_0 , we consider three different cases of BNS population models to sample potential BNS hosts. The host galaxies from filtered GLADE+ are chosen using these three different population models:

- $\langle M_{\star} \rangle = 10^9 M_{\odot}$,
- $\langle M_{\star} \rangle = 10^{10} M_{\odot}$,
- $\langle M_{\star} \rangle = 10^{11} M_{\odot}$.

We have considered these mass models by adopting the merger rate density distribution curve from Santoliquido et al. (2022) and shifting the pivotal point of the stellar mass. As explained in section 4.1, these mass models are log-normal distributions and are fitted using broken power law given by eq. 9 with the parameters given in table 1. The broken power law forms a PDF which then is combined with the normalized densities from Fig. 5 to sample potential BNS host galaxies from filtered GLADE+. The blue and orange curves in Fig. 3 are the PDFs corresponding to the parameters given in table 1. The third case (green curve) however, is not fitted with a broken power law because if the pivotal point is set at $10^{11} M_{\odot}$, the normalized density from Fig. 5 dominates the broken power law as there are less than 1% galaxies having $M_{\star} \geq 10^{11} M_{\odot}$. Hence, for $\langle M_{\star} \rangle = 10^{11} M_{\odot}$ case, we use a step function to restrict the population to masses $M_{\star} \geq 10^{11} M_{\odot}$.

Using this combined probability distribution on the stellar masses, we sample a population of 50 potential BNS host galaxies per mass

Parameter	$\langle M_{\star} \rangle = 10^9 M_{\odot}$	$\langle M_{\star} \rangle = 10^{10} M_{\odot}$
m_{break}	9	10
α_1	2.4	1.7
α_2	-3.4	-4.6
Δ	0.015	0.010

Table 1. Parameters for the broken power law distributions on stellar mass for the two of the three mass models used for sampling sources from the filtered GLADE+ catalog. The parameters for the third case are not included as it is fitted with a step function instead of a broken power law.

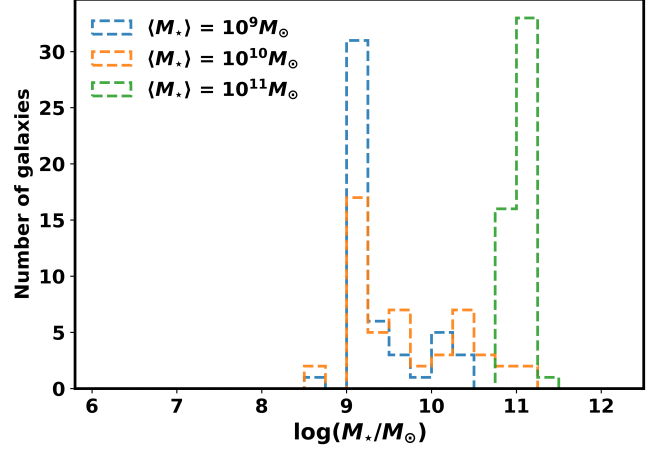


Figure 6. Distribution of the three populations of 50 sources chosen from the GLADE+ catalog with the population model discussed in section 4. This distribution represents galaxies chosen for parameter estimation in section 4.4.

model from the filtered GLADE+ catalog that follow the BNS merger rate model from Karathanasis et al. (2022) discussed in section 4.2. The corresponding distribution of the sampled galaxies for the three mass cases is shown in Fig. 6. Note that the $\langle M_{\star} \rangle = 10^{11} M_{\odot}$ population contains only high-mass galaxies and the use of the step function does not imply that the mean stellar mass of this population is $10^{11} M_{\odot}$. We use the symbol “ $\langle M_{\star} \rangle$ ” as a convention to denote the galaxy populations throughout this paper.

Thus, we have three populations of potential BNS host galaxies for the three $\langle M_{\star} \rangle$ cases. These three populations have their masses as discussed above, host redshifts that follow the merger rate model, and their peculiar velocity dispersion (σ_{v_p}) for individual galaxies. With these velocity dispersions and host galaxy redshift corrected for peculiar velocity we get the v_p realizations for each galaxy in every population.

4.4 Luminosity distance estimation for BNS sources

To estimate the value of the Hubble constant from these sources, we need an estimation of the luminosity distance for these mock BNS samples for all three different detector network configurations chosen in this analysis. To estimate the luminosity distance, we follow two different procedures, (i) we use the parameter estimation code Bilby for 10 BNS sources, and (ii) we estimate the posterior on the luminosity distance using a Gaussian approximation for 50 sources with a standard deviation equal to the median uncertainty on luminosity distance estimate from Bilby luminosity distance estimates. As we are using median errors on distance estimated from Bilby, we take into account the degeneracy with the inclination angle in a Gaussian

approximation. However, this approximation cannot capture the non-Gaussian nature of the posterior. However, on combining multiple GW sources (about 10 sources) for estimating H_0 , the posterior on Hubble constant H_0 will become Gaussian by central limit theorem. As a result, this approximation will not impact the conclusion significantly (this is discussed in detail later). We do not perform Bilby parameter estimation for 50 GW sources to reduce the computational cost.

Parameter estimation using Bilby: We perform parameter estimation of the GW sources using the Bilby (Ashton et al. 2019) package to get a realistic posterior on the luminosity distance for the BNSs for three different detector networks, namely:

- (i) LVK: LIGO-Livingston + LIGO-Hanford + Virgo + KAGRA
- (ii) LVKI: LVK + LIGO-India
- (iii) CE + ET: Cosmic Explorer + Einstein Telescope

To begin with, we first simulate BNS merger events in the chosen galaxies from the three galaxy populations from the GLADE+ catalog by injecting the GW source parameters $m_1, m_2, d_L, \theta_{JN}, \psi, \phi, \text{RA}$, and Dec. The parameters m_1 and m_2 denote the component masses randomly sampled from a uniform distribution over the range $[0.8 M_\odot, 2.5 M_\odot]$. The injected d_L is calculated using eq. 4 where $z_{\text{true}} \equiv z_{\text{CMB}}$ from GLADE+ and the injected value of H_0 is $70 \text{ km s}^{-1} \text{ Mpc}^{-1}$. The sky location of the injected GW source, given by the right ascension (RA) and declination (Dec), is obtained from the GLADE+ catalog. The injected values for the inclination angle θ_{JN} and the polarisation angle ψ are randomly sampled from uniform distributions over $[0, \pi]$ while that for the GW phase ϕ is sampled from uniform over $[0, 2\pi]$. We do not consider any spin effects like precession or tidal deformation in this analysis.

With these injection parameters, a GW signal waveform is generated using the IMRPhenomPv2 waveform model. With a sampling rate of 2GHz, the frequency domain waveform $h(f)$ is then added to the Gaussian colored noise $n(f)$ with the power spectral density $S_n(f)$ for the design sensitivity of LIGO, Virgo, KAGRA, LIGO-India, Cosmic Explorer, and Einstein Telescope. This generates the GW strain data for the injected source parameters. The data duration for each source for the LVK and LVKI cases is $\sim 15 - 20$ minutes varying with the randomly sampled component masses. The data duration for CE+ET case is $\sim 25 - 35$ minutes.

Since the luminosity distance d_L and the inclination angle θ_{JN} of the source are the only parameters of interest, we set the priors for all the other parameters as delta functions to expedite the parameter estimation. This approximation is appropriate as the luminosity distance and masses are not degenerate with these detector configurations. Luminosity distance and inclination angle are the maximally degenerate parameters, so we primarily consider these two for the parameter estimation. For d_L , the prior is uniform over $[1, 1000]$ Mpc, and the prior for θ_{JN} is sinusoidal from 0 to π . With a Gaussian likelihood over the parameter space, we use the nestle sampler in Bilby to estimate d_L and θ_{JN} . The d_L samples are obtained for 10 sources each from the three $\langle M_\star \rangle$ populations of BNS models for the three GW detector configurations LVK, LVKI, and CE+ET.

Parameter estimation using Gaussian method: We estimate the median σ_{d_L}/d_L for LVK, LVKI, and CE+ET from Bilby. Then we use that median error to model the Gaussian posterior on the luminosity distance for all the three cases of $\langle M_\star \rangle$. For LVK, LVKI, and CE+ET configuration, we consider the value of σ_{d_L}/d_L as 19%, 15.5% and 1.6% respectively. We generate d_L samples, for the entirety of the host populations from a Gaussian distribution with the mean obtained from eq. 4 and the percentage standard deviation obtained from the median values for every detector configuration. We then execute

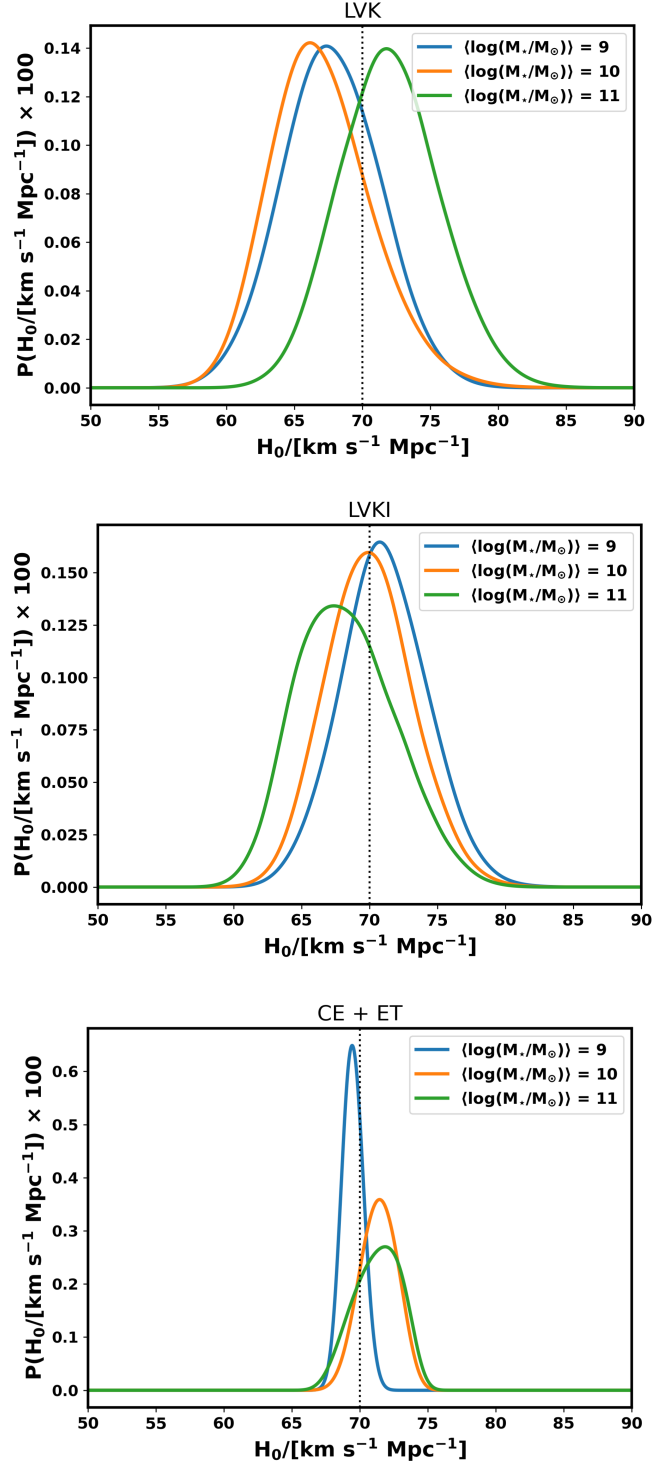


Figure 7. The combined posteriors of H_0 obtained for 10 simulated BNS merger events after correcting for the v_p bias for individual sources from the three BNS host populations from GLADE+. The three panels represent the combined H_0 posteriors for the three detector combinations. Each panel contains three posteriors for the three $\langle M_\star \rangle$ populations.

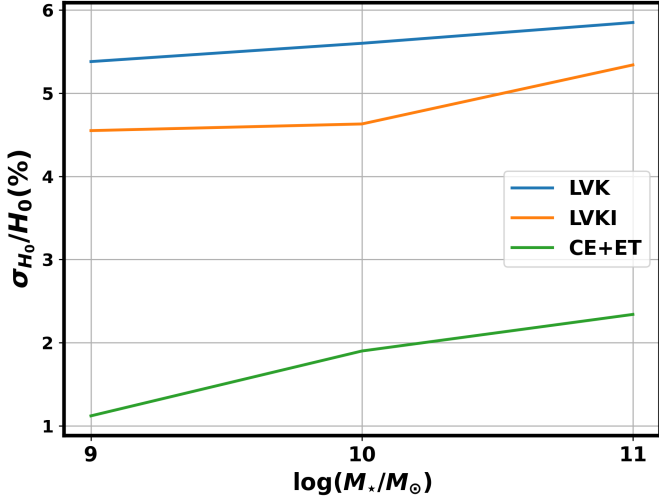


Figure 8. The precision on H_0 as a function of the log-stellar mass for the three detector configurations, obtained after combining posteriors from 10 BNS merger events, each simulated in the chosen population of galaxies from the GLADE+ catalog. The corresponding luminosity distance posteriors are obtained from parameter estimation.

the v_p correction formalism for all host galaxies each across three different detector configurations.

5 IMPACT OF PECULIAR VELOCITY ON HUBBLE CONSTANT ESTIMATION

As discussed in section 2, the peculiar motion of a galaxy contaminates the redshift estimate which affects the distance-redshift relation resulting in a biased inference of H_0 . Hence, Mukherjee et al. (2021b) developed a Bayesian formalism to incorporate and correct for the peculiar velocity contamination for inferring the Hubble constant from bright standard sirens. The equation for the framework is given by,

$$P(H_0 | \{D_{GW}\}, \{\hat{z}\}) \propto \prod_{n=1}^{N_{GW}} \int dd_L^n dv_p^n \mathcal{L}(d_L^n | H_0, v_p^n, z_n, \hat{u}_n, D_{GW}^n) P(z_n | \hat{u}_n) P(v_p^n | M, \hat{u}_n) \Pi(H_0), \quad (12)$$

where $P(H_0 | \{D_{GW}\}, \{\hat{z}\})$ is the posterior PDF of H_0 given the GW data for N_{GW} sources and their observed redshifts estimated from the EM counterpart; \mathcal{L} is the likelihood on the luminosity distance d_L which is assumed to be Gaussian; $P(z | \hat{u})$ is posterior of redshift estimate at source; $P(v_p | M, \hat{u})$ is the posterior of the peculiar velocity of the host galaxy that has a halo of mass M and located at sky position \hat{u} (RA, Dec); and $\Pi(H_0)$ is the prior on the value of H_0 .

Having three populations of galaxies (discussed in section 4.3) from GLADE+, we generate samples of v_p for each galaxy from a normal distribution with standard deviation σ_{v_p} . This forms the peculiar velocity posterior ($P(v_p | M, \hat{u})$). We then use the d_L posteriors obtained using (i) luminosity distance posterior from Bilby and (ii) Gaussian luminosity distance posterior to obtain posterior distribution on Hubble constant H_0 from the mock samples.

5.1 H_0 correction for GW sources with PE from Bilby

To implement the v_p correction (eq. 12), we use a flat prior on H_0 over the range $[20, 150] \text{ km s}^{-1} \text{ Mpc}^{-1}$, and with the d_L samples obtained using Bilby, we use the ensemble sampler from the emcee (Foreman-Mackey et al. 2013) package to implement the Metropolis-Hastings algorithm. The code samples from the above defined prior on H_0 and evaluate the likelihood by calculating the corresponding model value for d_L using the v_p realizations. After marginalizing over the v_p uncertainties, we get the corresponding H_0 samples and obtain the posterior probability distribution function for H_0 for individual sources using kernel smoothing with a scale of $\sim 0.013 \text{ km s}^{-1} \text{ Mpc}^{-1}$. We then normalize the 10 individual posteriors and combine them to obtain a combined H_0 posterior for each $\langle M_\star \rangle$ population for each detector configuration.

In Fig. 7 we present the combined posteriors for 10 sources from the three $\langle M_\star \rangle$ cases for LVK, LVKI and CE+ET detector configurations respectively. For the LVK configuration, the joint posteriors for the three populations have a similar spread. With the addition of the LIGO-India detector, as the uncertainty on the estimation of luminosity distance decreases, we start to see the impact of the stellar mass of the host galaxy on the precision of H_0 . This effect becomes more evident from the CE+ET configuration as it has the most precise d_L estimation of the three.

To elucidate the role of distance uncertainty, we plot the precision on H_0 as a function of the log of the expectation value of the host stellar mass for the three detector networks as shown in Fig. 8. We see that with the CE+ET detectors, for the $\langle M_\star \rangle = 10^9 M_\odot, 10^{10} M_\odot$ and $10^{11} M_\odot$ populations, the respective H_0 precisions are $\sim 1.1\%$, 1.9% and 2.3% . We observe that for CE+ET, as we go from low-mass BNS host galaxies to high-mass BNS host galaxies, the precision on H_0 inferred from a BNS merger in the host drops by a factor of ~ 2 .

Fig. 9 shows the precision on H_0 as a function of the number of bright siren events cumulatively combined for the three detector configurations, denoted by three different markers. For each marker, the red, yellow, and blue lines represent the $\langle M_\star \rangle = 10^9 M_\odot, 10^{10} M_\odot, 10^{11} M_\odot$ populations respectively. Here we see the interplay between the distance error and the peculiar velocity bias. With the CE+ET configuration, the contribution from the peculiar velocity uncertainty to the precision on H_0 far exceeds that from the distance uncertainty. Hence we clearly see the impact of the host properties in terms of the separation between the three dashed lines with lozenge (\blacklozenge) markers. As the $\langle M_\star \rangle = 10^{11} M_\odot$ population contains extremely heavy galaxies of the order of $10^{11} M_\odot - 10^{12} M_\odot$, the peculiar velocity contribution from the host galaxies in this population is much greater than that from the other two populations. As a result, the blue dashed line gets flattened at $N_{GW} = 3$ and the precision on H_0 does not improve even after combining 10 sources.

5.2 H_0 correction for GW sources with PE from Gaussian approximation

Before we perform an analysis of the entire chosen population of BNS host galaxies, we first compare the results from the non-Gaussian d_L posteriors with Gaussian ones. For the exact same sources, we make a plot, similar to Fig. 8 in Fig. 10. Comparing the similar colored lines from the two figures, we observe that with the Gaussian approximation with median percent standard deviation, the precision of H_0 for LVK and LVKI configurations is slightly poorer than that for the non-Gaussian d_L posteriors. For the CE+ET configuration, the Gaussian case shows a steeper slope from $\langle M_\star \rangle = 10^{10} M_\odot$ to $10^{11} M_\odot$. This assures that with the median σ_{d_L}/d_L , we are not

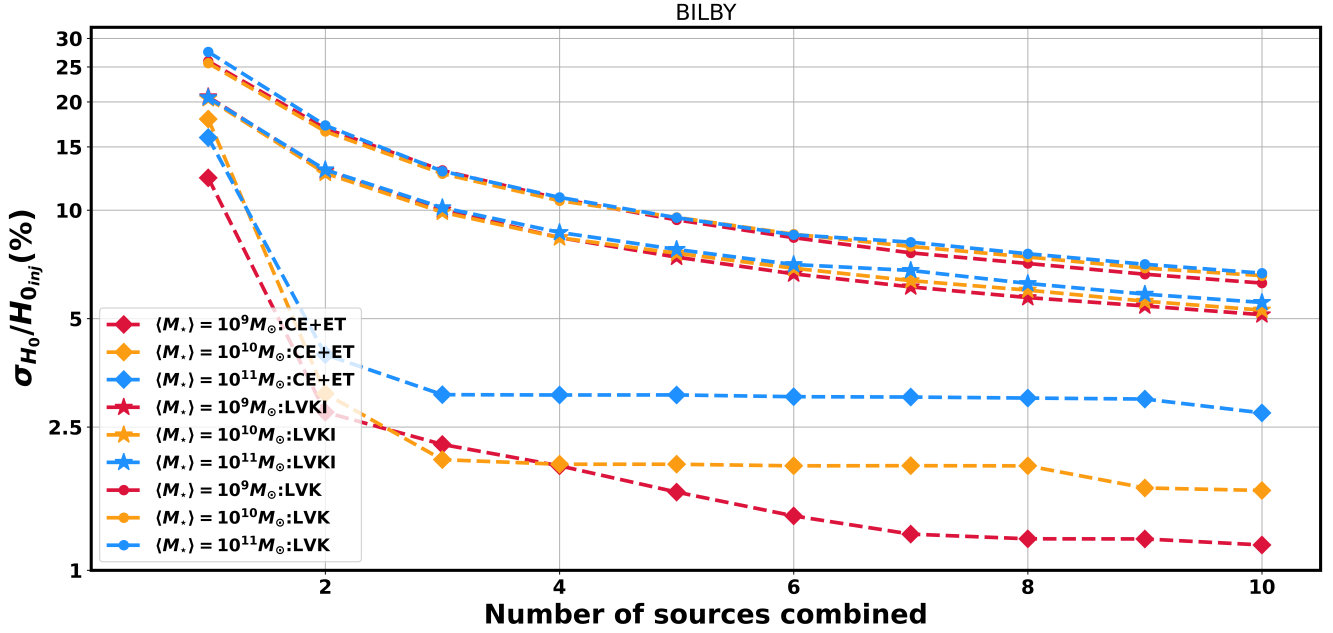


Figure 9. Precision on H_0 as a function of the number of sources cumulatively combined for the three detector configurations (denoted by distinct markers) for the three $\langle M_\star \rangle$ populations (distinctly colored). The distance posteriors are obtained from parameter estimation discussed in section 4.4.

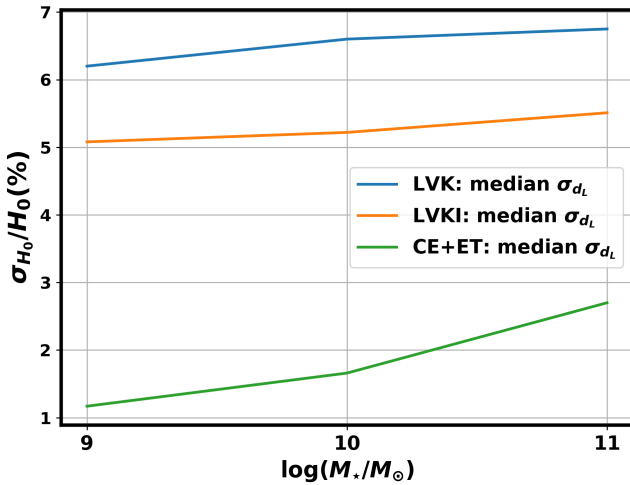


Figure 10. The precision on H_0 as a function of the log-stellar mass for the three detector configurations for the exact same sources as in Fig. 8. The luminosity distance samples are obtained from a Gaussian distribution with a standard deviation obtained from the median of the percent standard deviation for 30 sources (10 per population) per detector configuration.

underestimating the contribution from the distance uncertainty to the precision on H_0 .

Fig. 11 shows the precision on H_0 as a function of the number of bright siren events cumulatively combined (similar to Fig. 9 but with 50 sources), with Gaussian approximation for the luminosity distance with median σ_{d_L}/d_L for the three detector configurations. The three detector configurations are denoted by three different markers, similar to Fig. 9. For each marker, the red, yellow, and blue lines represent the $\langle M_\star \rangle = 10^9 M_\odot$, $10^{10} M_\odot$, $10^{11} M_\odot$ populations respectively. It can be seen that for the CE+ET configuration, for BNS host

galaxies with a stellar mass of the order of $10^9 M_\odot$, a one percent precision on H_0 can be attained with ≈ 15 bright siren events. If the host stellar mass is of the order $10^{10} M_\odot$, we need more than 20 events, and for $10^{11} M_\odot$, we need at least 50 bright siren events to reach the 1%-precision on H_0 . Similar to Fig. 9, we see that the blue lozenges in Fig. 11, representing the CE+ET configuration for the $\langle M_\star \rangle = 10^{11} M_\odot$ population, reach saturation and tend to get flattened as we combine more and more posteriors. As the peculiar velocity uncertainty far exceeds the distance error (1.6%), combining more posteriors accounts for the distance error and highlights the contribution from the host galaxy properties.

6 CONCLUSION AND FUTURE OUTLOOK

Binary neutron stars (BNS), being a class of bright standard sirens, are the ideal candidates to resolve the Hubble tension. However, since they are detected at low redshifts, the peculiar motions of their host galaxies contaminate the redshift and contribute significantly to the error budget on the inference of the Hubble constant (H_0). Hence to correct for the peculiar velocity contamination, it is necessary to estimate the peculiar velocity accurately. The peculiar velocity estimates are driven by the properties of the host galaxies of GW sources. Along with appropriate modeling of the source population, to discern the role of their host properties, we need to also analyze the impact of the distance uncertainty of a GW source on the H_0 estimation. Hence we considered three different ground-based detector configurations. These three configurations each lead to a different approximate uncertainty on the distance inferred from them.

With different detectors, we get different accuracy in the estimation of the luminosity distance of the GW sources. First, we consider the LIGO (Hanford and Livingston) - Virgo - KAGRA (LVK) network. We see that with LVK, the median uncertainty on the d_L estimate for 30 sources is 19%. If the d_L uncertainty exceeds $\sim 20\%$, the impact of v_p uncertainty is shrouded and $\sigma_{d_L}^2$ starts leading $\sigma_{H_0}^2$. $\sigma_{d_L}^2$ is

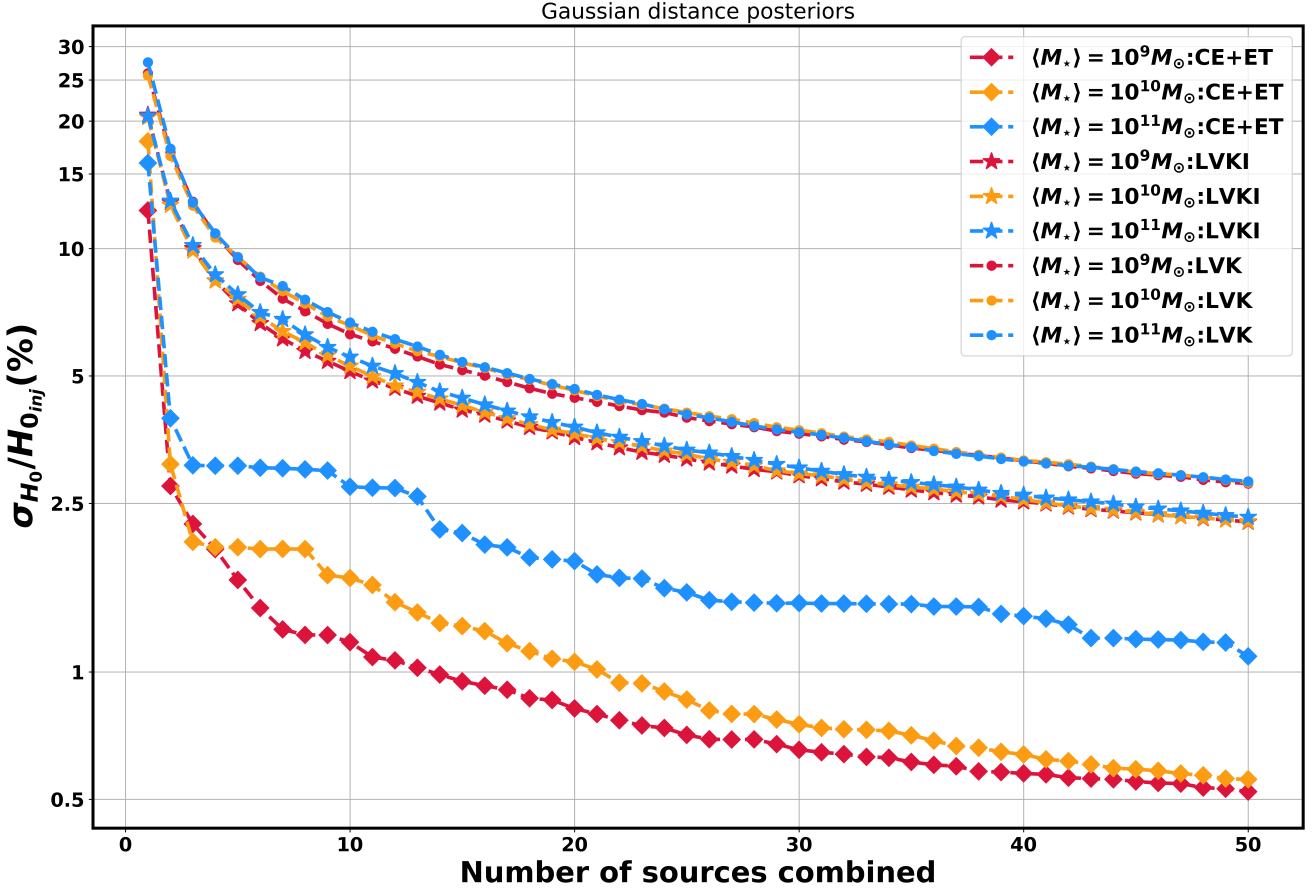


Figure 11. Precision on H_0 as a function of the number of sources cumulatively combined for the three detector configurations (denoted by distinct markers) for the three $\langle M_\star \rangle$ populations (distinctly colored). The distance posteriors are approximated with a Gaussian with percent standard deviation obtained from the median value (refer to section 5.2) for 10 sources for each detector configuration and each case.

largely dependent on the “loudness” of the GW chirp which depends on the intrinsic properties of the GW sources.

The signal-to-noise ratio (SNR) of a GW incident on a given detector can vary depending on the number of detectors. Hence to achieve greater accuracy on d_L , we consider another detector (LIGO-India) along with LVK. We observe that with the addition of the LIGO-India detector, we get a much better constraint on the d_L of the GW sources. The median uncertainty on the d_L estimate for the same 30 sources is 15.5%. The improved d_L estimates illuminate the contribution of v_p uncertainty and thus make way for the GW host property dependence to show up in the form of a significant difference in the H_0 precision for the BNS host populations.

To minimize the dominance of the error in the distance measurement, we considered a third configuration involving the Cosmic Explorer and Einstein Telescope (CE+ET) detectors. The CE+ET configuration has a median distance uncertainty of 1.6% which helps explore the host property dependence of peculiar velocity to its full potential.

The results from this study present a forecast on the impact of the host properties of GW sources, particularly BNSs on the peculiar velocity estimation and subsequently on the inference of H_0 . The results for these real galaxies from the GLADE+ catalog show that the stellar mass has a major impact on the peculiar velocity estimation and as a consequence, it significantly affects the inference of H_0 . To shed

light on the impact of the host properties on peculiar velocity estimation, we need to minimize the dominance of the distance uncertainty. We saw that a BNS merger event detected by CE+ET configuration located in a host galaxy with stellar mass $10^9 M_\odot$ yields a more precise estimate of H_0 by a factor of 2 than a host with stellar mass $10^{11} M_\odot$. This implies that host galaxies with more stellar mass will have a larger uncertainty on their peculiar velocity. The key takeaway is that it is equally important to measure the luminosity distance with greater accuracy as it is important to correct for the peculiar velocity of the GW source, to achieve precision measurement of the Hubble constant.

In conclusion, the variance on H_0 is an interplay between the luminosity distance uncertainties and the peculiar velocity uncertainties. Hence for a precise estimation of H_0 , it is necessary to accurately determine distances to GW sources while simultaneously estimating their peculiar velocities with precision. Lastly, we saw that by combining more sources, typically of the order of 50, we can reach a 1% precision on H_0 . However, this will depend on the host properties of the GW sources due to their peculiar velocity contamination. We saw that with CE+ET configuration, BNS mergers from less massive host galaxies will lead to a precision of 1% on H_0 with approximately 15 events as compared to 40-50 events for high mass galaxies. In the future, with accurate modeling of peculiar velocity and accurately mitigating its contamination, one can reach a 1% measurement with

CE+ET from 50-200 sources distributed up to $z = 0.05$ depending on the underlying population of the host galaxies. From LVK and LVKI one can achieve 3 – 2.5% measurement of the Hubble constant H_0 from 50 GW sources.

ACKNOWLEDGEMENTS

The authors thank Abhishek Sharma for reviewing the manuscript and providing useful comments as a part of the LIGO publication and presentation policy. This work is a part of the `<data|theory>` Universe-Lab which is supported by the TIFR and the Department of Atomic Energy, Government of India. The authors are thankful to Mr. Parag Shah for maintaining the computer cluster of the `<data|theory>` Universe-Lab. The authors would like to thank the LIGO-Virgo-KAGRA Scientific Collaboration for providing the noise curves. This research has made use of data or software obtained from the Gravitational Wave Open Science Center (gwopenscience.org), a service of LIGO Laboratory, the LIGO Scientific Collaboration, the Virgo Collaboration, and KAGRA. LIGO Laboratory and Advanced LIGO are funded by the United States National Science Foundation (NSF) as well as the Science and Technology Facilities Council (STFC) of the United Kingdom, the Max-Planck-Society (MPS), and the State of Niedersachsen/Germany for support of the construction of Advanced LIGO and construction and operation of the GEO600 detector. Additional support for Advanced LIGO was provided by the Australian Research Council. Virgo is funded, through the European Gravitational Observatory (EGO), by the French Centre National de Recherche Scientifique (CNRS), the Italian Istituto Nazionale di Fisica Nucleare (INFN) and the Dutch Nikhef, with contributions by institutions from Belgium, Germany, Greece, Hungary, Ireland, Japan, Monaco, Poland, Portugal, Spain. The construction and operation of KAGRA are funded by Ministry of Education, Culture, Sports, Science and Technology (MEXT), and Japan Society for the Promotion of Science (JSPS), National Research Foundation (NRF) and Ministry of Science and ICT (MSIT) in Korea, Academia Sinica (AS) and the Ministry of Science and Technology (MoST) in Taiwan. This material is based upon work supported by NSF’s LIGO Laboratory which is a major facility fully funded by the National Science Foundation. We acknowledge the use of the following packages in this work: Astropy ([Astropy Collaboration et al. 2013, 2018, 2022](#)), Bilby ([Ashton et al. 2019; LIGO Scientific Collaboration 2018; Wette 2020](#)), emcee: MCMC Hammer ([Foreman-Mackey et al. 2013](#)), Matplotlib ([Hunter 2007](#)), NumPy ([Harris et al. 2020](#)), Pandas ([pandas development team 2020](#)), SciPy ([Virtanen et al. 2020](#)), Seaborn ([Waskom 2021](#)).

DATA AVAILABILITY

The data underlying this article will be shared at the request to the corresponding author.

This paper has been typeset from a $\text{\TeX}/\text{\LaTeX}$ file prepared by the author.

REFERENCES

Aasi J., et al., 2015, *Class. Quant. Grav.*, 32, 074001
 Abbott B. P., et al., 2016a, *Phys. Rev. D*, 93, 112004
 Abbott B. P., et al., 2016b, *Phys. Rev. Lett.*, 116, 061102
 Abbott B. P., et al., 2017a, *Phys. Rev. Lett.*, 119, 161101
 Abbott B. P., et al., 2017b, *Nature*, 551, 85

Abbott B. P., et al., 2018, *Living Rev. Rel.*, 21, 3
 Abbott B. P., et al., 2020a, *Living Reviews in Relativity*, 23
 Abbott R., et al., 2020b, *Phys. Rev. Lett.*, 125, 101102
 Abbott B. P., et al., 2021a, *The Astrophysical Journal*, 909, 218
 Abbott R., et al., 2021b, *The Astrophysical Journal Letters*, 915, L5
 Abbott R., et al., 2023, *Astrophys. J.*, 949, 76
 Abdalla E., et al., 2022, *JHEAp*, 34, 49
 Acernese F., et al., 2014, *Classical and Quantum Gravity*, 32, 024001
 Adams C., Blake C., 2020, *Monthly Notices of the Royal Astronomical Society*, 494, 3275
 Adhikari R. X., et al., 2022, arXiv:2209.11726
 Akutsu T., et al., 2021, *PTEP*, 2021, 05A101
 Artale M. C., Mapelli M., Bouffanais Y., Giacobbo N., Spera M., Pasquato M., 2020, *Mon. Not. Roy. Astron. Soc.*, 491, 3419
 Ashton G., et al., 2019, *The Astrophysical Journal Supplement Series*, 241, 27
 Aso Y., Michimura Y., Somiya K., Ando M., Miyakawa O., Sekiguchi T., Tatsumi D., Yamamoto H., 2013, *Phys. Rev. D*, 88, 043007
 Astropy Collaboration et al., 2013, *A&A*, 558, A33
 Astropy Collaboration et al., 2018, *AJ*, 156, 123
 Astropy Collaboration et al., 2022, *apj*, 935, 167
 B. P. Abbott et al. 2020, *The Astrophysical Journal Letters*, 892, L3
 Bayes T., Price 1763, *Philosophical Transactions of the Royal Society of London*, 53, 370
 Boruah S. S., Hudson M. J., Lavaux G., 2021, *Mon. Not. Roy. Astron. Soc.*, 507, 2697
 Branchini E., et al., 1999, *Monthly Notices of the Royal Astronomical Society*, 308, 1
 Branchini E., Eldar A., Nusser A., 2002, *Monthly Notices of the Royal Astronomical Society*, 335, 53
 Bryan G. L., Norman M. L., 1998, *The Astrophysical Journal*, 495, 80
 Carrick J., Turnbull S. J., Lavaux G., Hudson M. J., 2015, *Monthly Notices of the Royal Astronomical Society*, 450, 317
 Chen H.-Y., Fishbach M., Holz D. E., 2018, *Nature*, 562, 545
 Chen H.-Y., Haster C.-J., Vitale S., Farr W. M., Isi M., 2022, *Mon. Not. Roy. Astron. Soc.*, 513, 2152
 Colberg J. M., et al., 2000, *Monthly Notices of the Royal Astronomical Society*, 319, 209
 Cuesta-Lazaro C., Li B., Eggemeier A., Zarrouk P., Baugh C. M., Nishimichi T., Takada M., 2020, *Monthly Notices of the Royal Astronomical Society*, 498, 1175
 Curti M., Mannucci F., Cresci G., Maiolino R., 2019, *Monthly Notices of the Royal Astronomical Society*, 491, 944
 Dalal N., Holz D. E., Hughes S. A., Jain B., 2006, *Phys. Rev. D*, 74, 063006
 Dálya G., et al., 2022, *Monthly Notices of the Royal Astronomical Society*, 514, 1403
 Davis M., Nusser A., Willick J. A., 1996, *The Astrophysical Journal*, 473, 22
 Davis M., Nusser A., Masters K. L., Springob C., Huchra J. P., Lemson G., 2011, *Monthly Notices of the Royal Astronomical Society*, 413, 2906
 Del Pozzo W., 2012, *Phys. Rev. D*, 86, 043011
 Diaz C. C., Mukherjee S., 2021, arXiv:2107.12787
 Evans M., et al., 2021a, arXiv: 2109.09882
 Evans M., et al., 2021b, A Horizon Study for Cosmic Explorer: Science, Observatories, and Community (arXiv:2109.09882)
 F Acernese et al. 2014, *Classical and Quantum Gravity*, 32, 024001
 Feeney S. M., Peiris H. V., Williamson A. R., Nissanke S. M., Mortlock D. J., Alsing J., Scolnic D., 2019, *Phys. Rev. Lett.*, 122, 061105
 Fishbach M., et al., 2019, *The Astrophysical Journal Letters*, 871, L13
 Foreman-Mackey D., Hogg D. W., Lang D., Goodman J., 2013, *Publications of the Astronomical Society of the Pacific*, 125, 306
 Fry J. N., Gaztanaga E., 1994, *The Astrophysical Journal*, 425, 1
 Gair J. R., et al., 2023, *Astron. J.*, 166, 22
 Gayathri V., et al., 2021, *Astrophys. J. Lett.*, 908, L34
 Genzel R., et al., 2015, *The Astrophysical Journal*, 800, 20
 Gray R., et al., 2020, *Phys. Rev. D*, 101, 122001
 Gregory M. H. e. a., 2010, *Classical and Quantum Gravity*, 27, 084006
 Hall E. D., Evans M., 2019, *Classical and Quantum Gravity*, 36, 225002
 Harris C. R., et al., 2020, *Nature*, 585, 357

- Harry G. M., LIGO Scientific Collaboration 2010, *Classical and Quantum Gravity*, 27, 084006
- He J.-h., 2019, *Phys. Rev. D*, 100, 023527
- Hinshaw G., et al., 2013, *The Astrophysical Journal Supplement Series*, 208, 19
- Holz D. E., Hughes S. A., 2005, *The Astrophysical Journal*, 629, 15
- Hotokezaka K., Nakar E., Gottlieb O., Nisanke S., Masuda K., Hallinan G., Mooley K. P., Deller A. T., 2018, A Hubble constant measurement from superluminal motion of the jet in GW170817 ([arXiv:1806.10596](https://arxiv.org/abs/1806.10596))
- Howlett C., Davis T. M., 2020, *Monthly Notices of the Royal Astronomical Society*, 492, 3803
- Hubble E., 1929, *Proceedings of the National Academy of Science*, 15, 168
- Hudson M. J., 1994, *Monthly Notices of the Royal Astronomical Society*, 266, 475
- Hudson M. J., Turnbull S. J., 2012, *The Astrophysical Journal Letters*, 751, L30
- Hudson M. J., Smith R. J., Lucey J. R., Branchini E., 2004, *Monthly Notices of the Royal Astronomical Society*, 352, 61
- Hunt L., et al., 2012, *Monthly Notices of the Royal Astronomical Society*, 427, 906
- Hunt L., Dayal P., Magrini L., Ferrara A., 2016, *Monthly Notices of the Royal Astronomical Society*, 463, 2020
- Hunter J. D., 2007, *Computing in Science & Engineering*, 9, 90
- Jasche Wandelt 2013, *Monthly Notices of the Royal Astronomical Society*, 432, 894
- Jasche, J. Lavaux, G. 2019, *Astronomy & Astrophysics*, 625, A64
- Kaiser N., Efstathiou G., Ellis R., Frenk C., Lawrence A., Rowan-Robinson M., Saunders W., 1991, *Monthly Notices of the Royal Astronomical Society*, 252, 1
- Karathanasis C., Revenu B., Mukherjee S., Stachurski F., 2022, GWSim: A python package to create GW mock samples for different astrophysical populations and cosmological models of binary black holes, [doi:10.48550/ARXIV.2210.05724](https://arxiv.org/abs/2210.05724), <https://arxiv.org/abs/2210.05724>
- Karathanasis C., Mukherjee S., Mastrogiovanni S., 2023, *Mon. Not. Roy. Astron. Soc.*, 523, 4539
- Kauffmann G., et al., 2003a, *Monthly Notices of the Royal Astronomical Society*, 341, 33
- Kauffmann G., et al., 2003b, *Monthly Notices of the Royal Astronomical Society*, 341, 54
- Kauffmann G., White S. D. M., Heckman T. M., Ménard B., Brinchmann J., Charlot S., Tremonti C., Brinkmann J., 2004, *Monthly Notices of the Royal Astronomical Society*, 353, 713
- Kewley L. J., Ellison S. L., 2008, *The Astrophysical Journal*, 681, 1183
- Kim A. G., Linder E. V., 2020, *Phys. Rev. D*, 101, 023516
- LIGO Scientific Collaboration 2018, LIGO Algorithm Library - LALSuite, free software (GPL), [doi:10.7935/GT1W-FZ16](https://arxiv.org/abs/10.7935/GT1W-FZ16)
- Lavaux G., Hudson M. J., 2011, *Monthly Notices of the Royal Astronomical Society*, 416, 2840
- Lavaux G., Jasche J., 2015, *Monthly Notices of the Royal Astronomical Society*, 455, 3169
- Lemaître G., 1927, *Annales Soc. Sci. Bruxelles A*, 47, 49
- Lemaître A. G., Eddington A. S., 1931, *Monthly Notices of the Royal Astronomical Society*, 91, 490
- Leyde K., Mastrogiovanni S., Steer D. A., Chassande-Mottin E., Karathanasis C., 2022, *JCAP*, 09, 012
- Ma Y.-Z., Branchini E., Scott D., 2012, *Monthly Notices of the Royal Astronomical Society*, 425, 2880
- Madau P., Dickinson M., 2014, *Annual Review of Astronomy and Astrophysics*, 52, 415
- Maggiore M., 2007, *Gravitational Waves: Volume 1: Theory and Experiments*. Oxford University Press, [doi:10.1093/acprof:oso/9780198570745.001.0001](https://doi.org/10.1093/acprof:oso/9780198570745.001.0001), <https://doi.org/10.1093/acprof:oso/9780198570745.001.0001>
- Maggiore M., et al., 2020, *JCAP*, 03, 050
- Magnelli, B. et al., 2012, *A&A*, 539, A155
- Maiolino, R. et al., 2008, *A&A*, 488, 463
- Mannucci F., et al., 2009, *Monthly Notices of the Royal Astronomical Society*, 398, 1915
- Mannucci F., Cresci G., Maiolino R., Marconi A., Gnerucci A., 2010, *Monthly Notices of the Royal Astronomical Society*, 408, 2115
- Mannucci F., Salvaterra R., Campisi M. A., 2011, *Monthly Notices of the Royal Astronomical Society*, 414, 1263
- Mastrogiovanni S., et al., 2021a, *Phys. Rev. D*, 104, 062009
- Mastrogiovanni S., Duque R., Chassande-Mottin E., Daigne F., Mochkovitch R., 2021b, *Astronomy and Astrophysics - A&A*, 652, A1
- Mooley K. P., et al., 2018a, *Nature*, 561, 355
- Mooley K. P., et al., 2018b, *The Astrophysical Journal Letters*, 868, L11
- Mortlock D. J., Feeney S. M., Peiris H. V., Williamson A. R., Nisanke S. M., 2019, *Phys. Rev. D*, 100, 103523
- Mukherjee S., et al., 2020a, First measurement of the Hubble parameter from bright binary black hole GW190521 ([arXiv:2009.14199](https://arxiv.org/abs/2009.14199))
- Mukherjee S., Wandelt B. D., Silk J., 2020b, *Mon. Not. Roy. Astron. Soc.*, 494, 1956
- Mukherjee S., Wandelt B. D., Nisanke S. M., Silvestri A., 2021a, *Phys. Rev. D*, 103, 043520
- Mukherjee S., Lavaux G., Bouchet F. R., Jasche J., Wandelt B. D., Nisanke S., Leclercq F., Hotokezaka K., 2021b, *A&A*, 646, A65
- Mukherjee S., Krolewski A., Wandelt B. D., Silk J., 2022, [arXiv:2203.03643](https://arxiv.org/abs/2203.03643)
- Napolitano N. R., et al., 2020, *MNRAS*, 498, 5704
- Nguyen N.-M., Schmidt F., Lavaux G., Jasche J., 2021, *Journal of Cosmology and Astroparticle Physics*, 2021, 058
- Nicolaou C., Lahav O., Lemos P., Hartley W., Braden J., 2020, *Monthly Notices of the Royal Astronomical Society*, 495, 90
- Nisanke S., Holz D. E., Hughes S. A., Dalal N., Sievers J. L., 2010, *The Astrophysical Journal*, 725, 496
- Nisanke S., Kasliwal M., Georgieva A., 2013, *The Astrophysical Journal*, 767, 124
- Nusser A., Da Costa L. N., Branchini E., Bernardi M., Alonso M., Wegner G., Willmer C. N. A., Pellegrini P. S., 2001, *Monthly Notices of the Royal Astronomical Society*, 320, L21
- Oguri M., 2016, *Phys. Rev. D*, 93, 083511
- Palmese A., et al., 2020, *The Astrophysical Journal Letters*, 900, L33
- Palmese A., Bom C. R., Mucesh S., Hartley W. G., 2023, *The Astrophysical Journal*, 943, 56
- Perna R., Artale M. C., Wang Y.-H., Mapelli M., Lazzati D., Sgalletta C., Santoliquido F., 2022, *Mon. Not. Roy. Astron. Soc.*, 512, 2654
- Pike R., Hudson M. J., 2005, *The Astrophysical Journal*, 635, 11
- Planck Collaboration 2020, *Astronomy & Astrophysics*, 641, A6
- Planck Collaboration et al., 2014, *A&A*, 571, A16
- Planck Collaboration et al., 2016, *A&A*, 594, A13
- Planck Collaboration et al., 2021, *A&A*, 652, C4
- Punturo M., et al., 2010, *Classical and Quantum Gravity*, 27, 194002
- Radburn-Smith D. J., Lucey J. R., Hudson M. J., 2004, *Monthly Notices of the Royal Astronomical Society*, 355, 1378
- Reitze D., et al., 2019, in *Bulletin of the American Astronomical Society*, p. 35 ([arXiv:1907.04833](https://arxiv.org/abs/1907.04833)), [doi:10.48550/arXiv.1907.04833](https://arxiv.org/abs/1907.04833)
- Riess A. G., et al., 2022, *The Astrophysical Journal Letters*, 934, L7
- Ronchini S., et al., 2022, *Astronomy & Astrophysics*, 665, A97
- Saleem M., et al., 2022, *Class. Quant. Grav.*, 39, 025004
- Sanders R. L., et al., 2019, *Monthly Notices of the Royal Astronomical Society*, 491, 1427
- Santoliquido F., Mapelli M., Artale M. C., Boco L., 2022, *Monthly Notices of the Royal Astronomical Society*, 516, 3297
- Santoliquido F., Mapelli M., Iorio G., Costa G., Glover S. C. O., Hartwig T., Klessen R. S., Merli L., 2023, [arXiv:2303.15515](https://arxiv.org/abs/2303.15515)
- Schutz B., 1986, *Nature*, 323, 310
- Shaya E. J., Tully R., Pierce M. J., 1992, *The Astrophysical Journal*, 391, 16
- Sheth Diaferio 2001, *Monthly Notices of the Royal Astronomical Society*, 322, 901
- Soares-Santos M., et al., 2019, *The Astrophysical Journal Letters*, 876, L7
- Sohn J., Geller M. J., Zahid H. J., Fabricant D. G., Diaferio A., Rines K. J., 2017, *ApJS*, 229, 20
- Song Y.-S., Percival W. J., 2009, *Journal of Cosmology and Astroparticle Physics*, 2009, 004

- Taylor E. N., et al., 2011, [Monthly Notices of the Royal Astronomical Society](#), 418, 1587
- The LIGO Scientific Collaboration et al., 2022, The population of merging compact binaries inferred using gravitational waves through GWTC-3 ([arXiv:2111.03634](#))
- Tremonti C. A., et al., 2004, [The Astrophysical Journal](#), 613, 898
- Turnbull S. J., Hudson M. J., Feldman H. A., Hicken M., Kirshner R. P., Watkins R., 2012, [Monthly Notices of the Royal Astronomical Society](#), 420, 447
- Turner R. J., Blake C., Ruggeri R., 2022, [Monthly Notices of the Royal Astronomical Society](#), 518, 2436
- Unnikrishnan C. S., 2013, [International Journal of Modern Physics D](#), 22, 1341010
- Virtanen P., et al., 2020, [Nature Methods](#), 17, 261
- Waskom M. L., 2021, [Journal of Open Source Software](#), 6, 3021
- Wechsler R. H., Tinker J. L., 2018a, [ARA&A](#), 56, 435
- Wechsler R. H., Tinker J. L., 2018b, [Ann. Rev. Astron. Astrophys.](#), 56, 435
- Wette K., 2020, [SoftwareX](#), 12, 100634
- Wong K. C., et al., 2019, [Monthly Notices of the Royal Astronomical Society](#), 498, 1420
- Zahid H. J., Dima G. I., Kudritzki R.-P., Kewley L. J., Geller M. J., Hwang H. S., Silverman J. D., Kashino D., 2014, [The Astrophysical Journal](#), 791, 130
- Zheng Y., Zhang P., Jing Y., Lin W., Pan J., 2013, [Phys. Rev. D](#), 88, 103510
- pandas development team T., 2020, pandas-dev/pandas: Pandas, [doi:10.5281/zenodo.3509134](https://doi.org/10.5281/zenodo.3509134), <https://doi.org/10.5281/zenodo.3509134>